Detailed numerical modelling of moist air flow through a complex airtightness defect

Clément Belleudy[*,1,2], Monika Woloszyn[1], Matthieu Cosnier[2]

1 LOCIE, CNRS 5271, Université Savoie Mont Blanc
Campus Scientifique Savoie Technolac
Bâtiment Helios, Avenue du Lac Léman,
73376 Le Bourget du Lac, France

2 Centre Scientifique et Technique du Bâtiment
24 rue Joseph Fourier
38400 Saint Martin d'Hères, France
**Corresponding author: clement.belleudy@cstb.fr*

ABSTRACT

Mastering building airtightness is essential to meet the requirements of current and future building codes, not only for saving energy but also for ensuring moisture safety. Perfect airtightness is difficult to achieve: failures are often observed, due to bad design or poor workmanship. Some published investigations proved that leaking air mostly flows through porous material and thin air channels, due to material imperfections and construction tolerances. In addition, air inlet and outlet are not necessarily close to each other, which makes air leakage paths through the building envelope multidimensional and difficult to map. Very few existing models enable such complex air leakage geometries to be dealt with.
In this article, a recently developed detailed model coupling heat air and moisture (HAM) transfer is presented and used to analyse moist air flows due to airtightness defects. The model is able to deal with anisothermal airflow through complex 2D building assemblies, including both air permeable porous materials and thin air channels. The model is then applied on a 2D air leakage configuration subjected to infiltration and exfiltration scenarii. Results are analysed in terms of moisture risk and energy impact. A parametric study on boundary conditions is carried out. The results show higher moisture risk in case of air exfiltration through the airtightness defect.

KEYWORDS

HAM, air leakage, moisture, airtightness, modelling

1 INTRODUCTION

Building airtightness is a major issue to meet the targeted requirements of low energy buildings. Bad design and poor workmanship can lead to unintended air leakage across building envelopes, which leads not only to an increase in energy consumption, but also to additional potential moisture damages inside building assemblies. It is of importance to better assess the impact of air leakage on the hygrothermal performance of the envelope. There is a need to provide quantitative results of this impact in terms of energy and moisture, which may contribute to raise building actors' awareness about a better integration of airtightness into the building construction process.
Modelling coupled heat, air and moisture transfer is a demanding task, especially as leaking air flows through the building envelope by combined air channels and air permeable porous insulation materials. Moreover, these air paths are multidimensional and difficult to map. Measurement campaigns conducted in France on a sample of buildings enabled to locate most

frequently encountered air leakage (CETE de Lyon 2010). From these campaigns, booklets presenting 2D sections of the sensitive points towards air leakage have been released for main typologies of buildings. To the best of our knowledge, there are in literature very few numerical models able to deal with anisothermal HAM transfer through air permeable porous material and thin air channels. For example, a simplified approach to model HAM transfer in thin air channels in contact with airtight materials has been introduced by (Nespoli, Janetti, and Ochs 2013). In this "line source approach", air channels are reduced to 1D domains for HAM transfer and the coupling with HM transfer through airtight porous material is ensured by using heat and moisture surface film coefficients along the air channel. This approach has been successfully compared to experimental data (Janetti 2014). To deal with complex assemblies including air channels and air permeable porous insulating materials, (Janssens 1998) and (Langmans 2013) solve the velocity field in both domains: with Darcy law in the porous medium, and averaged Poiseuille law in the air channel. Similarly to Janetti, HAM transfer between porous and air domains are solved with a two-domain approach, meaning that both porous and air domains are coupled with surface coefficients.
In the present article, we use a newly-developed model called HAM-Lea ("Lea" standing for "Leakage"). It differs from the previous model by considering a one-domain approach - also called conjugate approach - to simulate HAM transfer in porous and air domains. Practically, the same structure of equations is used in both domains, and no surface coefficient is therefore required for the coupling. This model has been built from a HA-model (Belleudy et al. 2014) in which moisture has been subsequently implemented. This paper firstly presents HAM-Lea's governing equations, before applying it to a 2D airtightness defect in infiltration or exfiltration with transient temperature and moisture boundary conditions. In a third part, the impact of airflow on the building assembly is analysed in terms of moisture and energy, and the consequence on the results of a higher external maximal temperature is investigated.

2 NUMERICAL MODEL

2.1 Governing equations

HAM-Lea is formulated using the continuous medium approximation: material properties and local fields are averaged over Representative Elementary Volumes (REV), which enable conservation laws to be written in their local form using Partial Derivative Equations (PDE). HAM-Lea's conservation equations for energy (eq. 1), moisture (eq. 2), mass (eq. 3), and momentum (eq. 4) are given below, with $(T;\varphi;u;P)$ as variables:

$$\frac{\partial H(T;\varphi)}{\partial t} = -\nabla\cdot[q_{cond}(T;\varphi) + q_{conv}(T) + q_{lat}(T;\varphi)] \quad (1)$$

$$\frac{\partial w(\varphi)}{\partial t} = -\nabla\cdot[g_{diff}(T;\varphi) + g_{adv}(T;\varphi) + g_{liq}(\varphi)] \quad (2)$$

$$\nabla\cdot u = 0 \quad (3)$$

$$u = -\frac{k_{mat}}{\mu_{air}}\nabla P \quad (4)$$

The simple form of continuity equation (eq. 3) is due to low air velocities encountered in building physics, implying the assumption of incompressible flow. Darcy law (eq. 4) is a simplified form of Navier-Stokes equation in the porous material to describe momentum conservation. Averaged Poseuille law written in the air channel allows to identify an equivalent permeability (Belleudy 2015). Darcy law is valid for low velocities, i.e. a pore Reynolds number of order of unity. Natural convection is said to be of limited importance when indoor-outdoor temperature differences do not exceed 40°C (Langlais, Arquis, and McCaa 1990). As HAM-Lea is firstly dedicated for temperate climates, natural convection is not implemented. This choice also enhances simulation performance because Darcy law can be solved independently, prior to moisture and energy equations. For the energy equation, a

one-temperature approach is adopted, assuming therefore thermal equilibrium between air and solid material. This approximation is valid for building insulation materials with low air velocities, as proved by (Buchanan and Sherman 2000). In the energy equation (eq. 1), the enthalpy variation rate of a REV containing porous material is expressed as:

$$\frac{\partial H(T;\varphi)}{\partial t} = [\rho_{mat} c_{mat} + w(\varphi) c_w] \frac{\partial T}{\partial t} \quad (5)$$

A similar term can be written for REV in air channels (Belleudy 2015). The energy variation is driven by three net heat fluxes (q_{lat}, explained at the end of this section, q_{cond} and q_{conv}) as shown in (eq. 1). The heat conduction flux density q_{cond} is described by the well-known Fourier law (eq. 6) with a moisture dependent thermal conductivity $\lambda_{mat}(\varphi)$ in the porous material and a constant one λ_{air} in the air channel:

$$q_{cond}(T;\varphi) = -\lambda_{mat}(\varphi) \nabla T \quad (6)$$

Air is regarded as an ideal mixture between dry air and water vapour following the ideal gas law. The expression of the convective dry air flux density appearing in (eq. 1) is:

$$q_{conv}(T) = \rho_{air} c_{p_{air}} u T \quad (7)$$

Moisture conservation states that the increase rate of moisture content *w* in an REV is equal to the sum of three net moisture fluxes which are vapour diffusion, vapour advection and liquid transport. Vapour diffusion is described by Fick law (eq. 8). Vapour advection refers to the vapour flow carried by airflow (eq. 9). The humidity by volume of air, ρ_{vap}, can be linked with temperature and vapour pressure via the ideal gas law (eq. 11). Liquid transport is driven by capillary suction in water filled pores. This phenomena occurs in smaller pores first, and becomes dominant for high relative humidities ($\varphi > 0.98$). It can be written with φ as potential (eq. 10). g_{liq} is zero in air channels. The definition of relative humidity is needed (eq. 12) in order to add the relationship between φ and vapour pressure p_v, introducing the saturation pressure P_{sat}.

$$g_{diff}(T;\varphi) = -\delta_{mat}(\varphi) \nabla p_v(T;\varphi) \quad (8)$$

$$g_{adv}(T;\varphi) = \rho_{vap}(T;\varphi) u \quad (9)$$

$$g_{liq}(\varphi) = -D_w(\varphi) \frac{\partial w(\varphi)}{\partial} \nabla \varphi \quad (10)$$

$$\rho_{vap}(T;\varphi) = \frac{M_w}{RT} p_v(T;\varphi) \quad (11)$$

$$p_v(T;\varphi) = \varphi P_{sat}(T) \quad (12)$$

The latent heat flux density q_{lat} describes the latent heat transfer due to moisture sorption and desorption in the porous medium. This flux is the sum of a diffusive and an advective part (eq. 13). The sensible heat carried by liquid and vapour fluxes is commonly neglected toward the latent part in calculations (Künzel 1995).

$$q_{lat}(T;\varphi) = q_{lat\_diff}(T;\varphi) + q_{lat\_adv}(T;\varphi) = L_v g_{diff}(T;\varphi) + L_v g_{adv}(T;\varphi) \quad (13)$$

HAM-Lea outputs have been successfully compared with 1D numerical benchmarks from HAMSTAD project and with 2D experimental measurements (Belleudy 2015).

2.2 Boundary conditions

For air transfer, relative pressure is imposed at air inlets and a reference pressure at air outlets. The scalar product between air velocity and the outward-pointing normal vector *n* is set to zero on airtight boundaries. Boundary conditions for moisture transfer consist of relative humidity at air inlets and an inward imposed vapour diffusion flux at air outlets. This latter condition also holds for airtight but vapour permeable interfaces.

$$-n \cdot g_{surf} = \beta_{amb}(p_{v\_amb} - p_{v\_surf}) \quad (14)$$

Vapour tight boundaries are affected with a normal moisture flux equal to zero. Heat transfer boundary conditions consists of an imposed temperature at air inlets, an imposed inward heat

flux at air oulet considering a sensible part due to the convective thermal resistance and a latent part due to moisture diffusion. This latter condition also holds for airtight but non-adiabatic interfaces:

$$-\vec{n}\cdot\vec{q}_{surf} = h_{amb}(T_{surf} - T_{amb}) + L_v^{-}{}_{amb}(p_{v\,surf} - p_{v\,amb}) \quad (15)$$

Adiabatic boundary condition is a normal heat flux set to zero.

3 APPLICATION TO AN AIR LEAKAGE CONFIGURATION

3.1 Presentation of the case study

In this section, the numerical model is used to investigate the impact of coupled heat air and moisture transfer on a real-like air leakage geometry (fig. 1). It has been drawn from the previously mentioned measurement campaigns, which aimed to identify locations of wooden frame envelopes often subjected to air leakage.

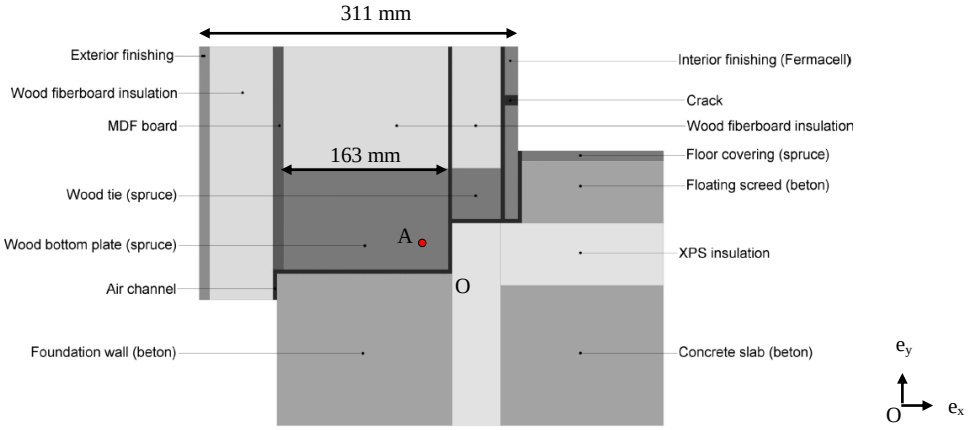

Figure 1: 2D section of the studied airtightness defect.
The point A (-30mm, 30mm) indicated above is used in section 4 to analyse the results.

Consequently to poor workmanship on the junction between wood bottom plate and foundation wall, flexible joints may be overlooked and the vapour barrier not sealed properly, which allows air to flow through the assembly via a thin air channel. To facilitate the modelling, it is assumed that no flexible joint remains, and the vapour barrier is removed to reproduce the effect of strong sealing discontinuities. The air computational domain is constituted by the 2mm air channel, the first layer of wood fiberboard insulation ($k_{mat} = 2.8\ 10^{-10}$ m^2) located behind the interior finishing, and a 10 mm diameter crack. The second and third layer of wood fiberboard insulation have been considered as airtight as they are not directly subjected to pressure gradient.

Table 1: Summary of the material properties. The readers are referred to the Fraunhofer IBP database, available in WUFI software, for a comprehensive description of the sorption isotherms and material properties

	μ factor [-]	λ_{mat} (φ=0.8) [W/(m.K)]	D_w (φ=0.8) [m^2/s]	c_{mat} [J/(kg.K]	ρ_{mat} [kg/m^3]
Beton C12/15	92	1.91	217 10^{-12}	850	2200
Fermacell	16	0.32	160 10^{-12}	1200	1153
Wood fiberboard	3	0.045	200 10^{-12}	2000	155
MDF board	12	0.12	0.0745 10^{-12}	2000	528
Spruce	4.3	0.28	53.3 10^{-12}	1500	455
XPS	100	0.03	Not cap. active	1500	40
Ext. finishing	8.1	0.93	0.130 10^{-12}	850	1360

3.2 Simulation scheme

This building assembly will be subjected to transient boundary conditions in both temperature and humidity. As we are mostly interested in long term behaviour, we use boundary

conditions with yearly variations from WUFI database (fig. 2). Indoor temperature oscillates between 20°C in winter and 22°C in summer, whereas outdoor temperature ranges from 0°C in winter to 18°C in the summer. Humidity by volume is higher indoors than outdoors, but this tendency is reversed for relative humidity because of lower outdoor temperature.

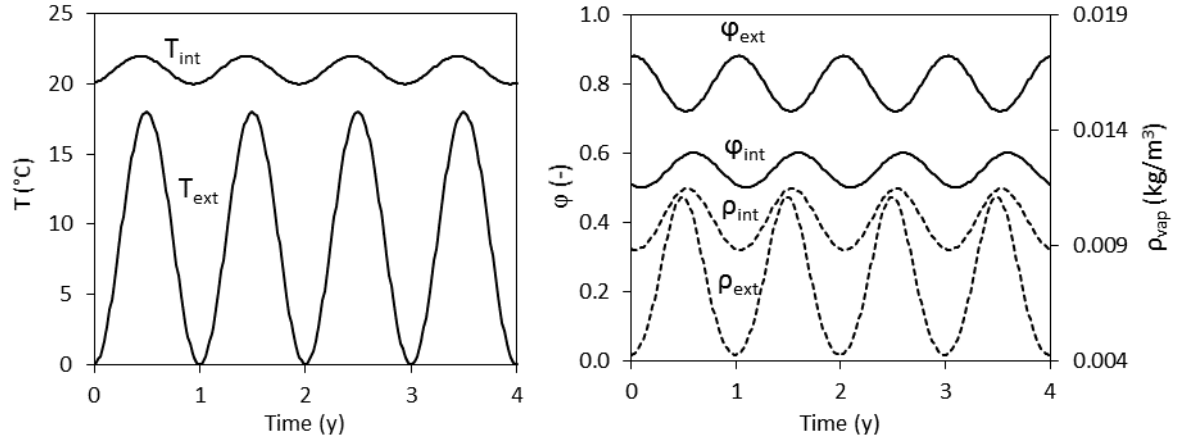

Figure 2: Yearly temperature (left) and humidity profiles (right) used as boundary conditions

In this study, both infiltration and exfiltration scenarii will be tested. For each scenario, two pressure differentials are tested – 0.1 Pa and 1 Pa – generating two airflow rates of 0.04 m^3/h and 0.4 m^3/h, respectively. The simulation scheme consists of one year of HM simulation (without airflow) used for initializing three-year HAM simulations. A 4-year HM simulation is also performed to make a comparison.

4 RESULTS AND DISCUSSION

4.1 Moisture

The impact of airflow on moisture field will be analysed by considering two indicators in a particularly sensible region: the averaged moisture content of the wood bottom plate w_{avg} and the moisture content evaluated at point A, noted w_A (see fig. 1).

It is shown on (fig. 3) that without airflow, the wood bottom plate only needs one year to reach hygric equilibrium, whereas two years are required in case of air leakage (infiltration or exfiltration). Observed tendencies differ in infiltration and exfiltration. When air infiltrates, w_{avg} decreases, indicating that the airflow dries up the assembly (fig. 3, left). As outdoor air is preheated in the assembly, air relative humidity decreases, hence it takes moisture from the assembly. On the contrary, a humidification occurs when air exfiltrates (fig. 3, right). Hot humid air is cooled down in the assembly, which increases its relative humidity and cause possible interstitial condensation if the dew point is reached. It also appears that the humidification process is more marked than the drying one for similar flowrates. This is firstly due to the non-linearity of the sorption curve (the more humid the material, the higher its hygric capacity) – and secondly to the additional liquid capillary flux becoming significant for high relative humidities. By drawing together with mean moisture contents the temperature difference between indoors and outdoors $¢T = T_{int} ¡ T_{ext}$ we get information on how fast the hygrothermal field reacts to boundary conditions. Maximum moisture risks are expected for high $¢T$. It may be noted that without airflow, the maximum moisture content is attained about three months after the maximum $¢T$ (20°C). In exfiltration for $¢P = 1$ Pa, this period is halved. Similar tendency is also observed in infiltration but to a lesser degree. This can be physically explained because without airflow, moisture is transferred exclusively by diffusion, whereas imposed airflow creates moisture advection which intensifies moisture migration. More local hygrothermal behaviour can be captured

considering moisture content at a point A (fig. 4). These plots show that the hygrothermal field of the wood bottom plate is much more impacted in the vicinity of the air channel.

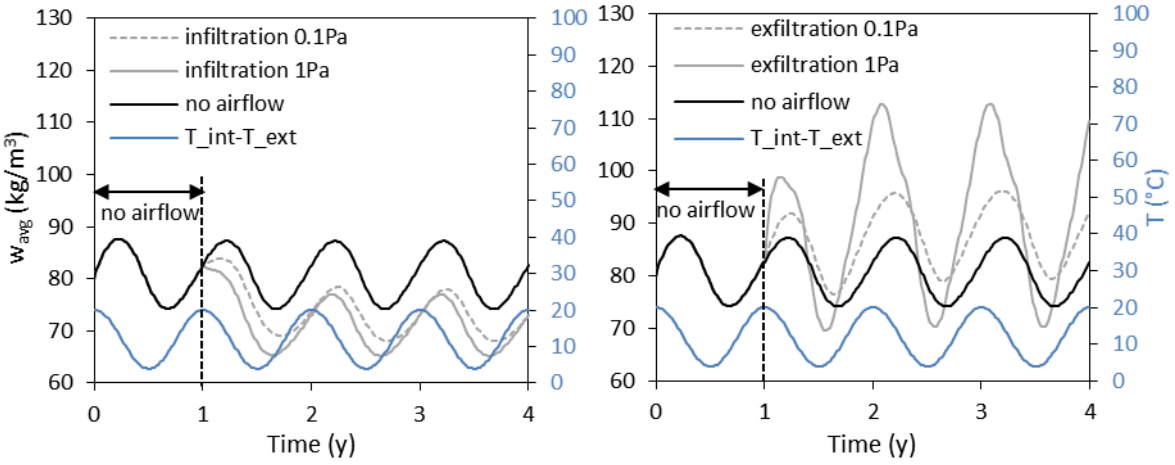

Figure 3 : Averaged moisture content of wood bottom plate for air infiltration (left) and exfiltration (right), over 4 years. The temperature difference between indoor and outdoor spaces is plotted in blue.

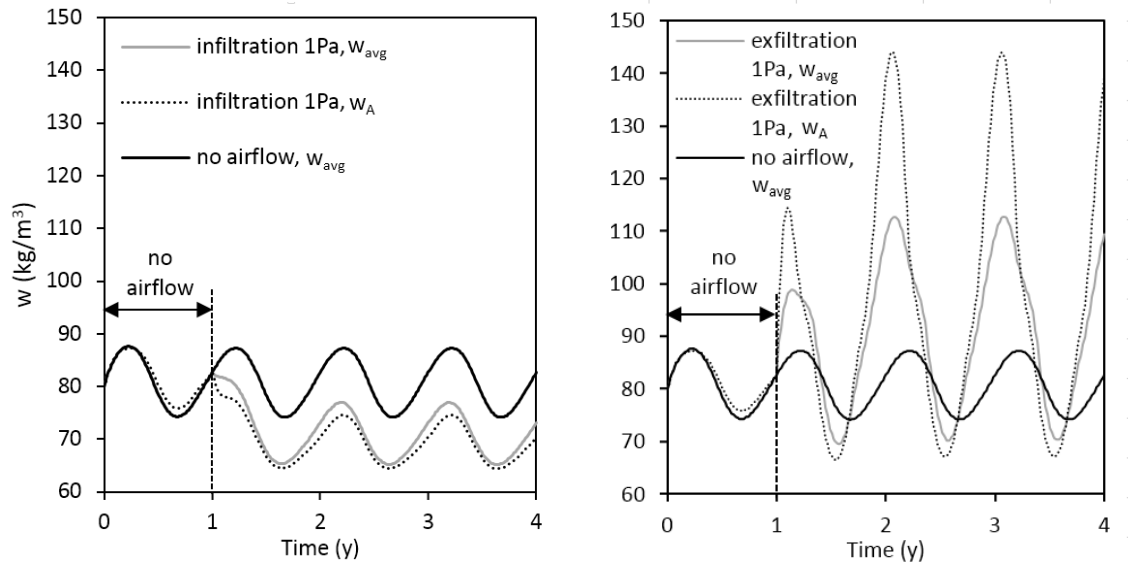

Figure 4: Comparison between averaged moisture content of wood bottom plate and ponctual moisture content evaluated at point A, for infiltrating and exfiltrating scenario.

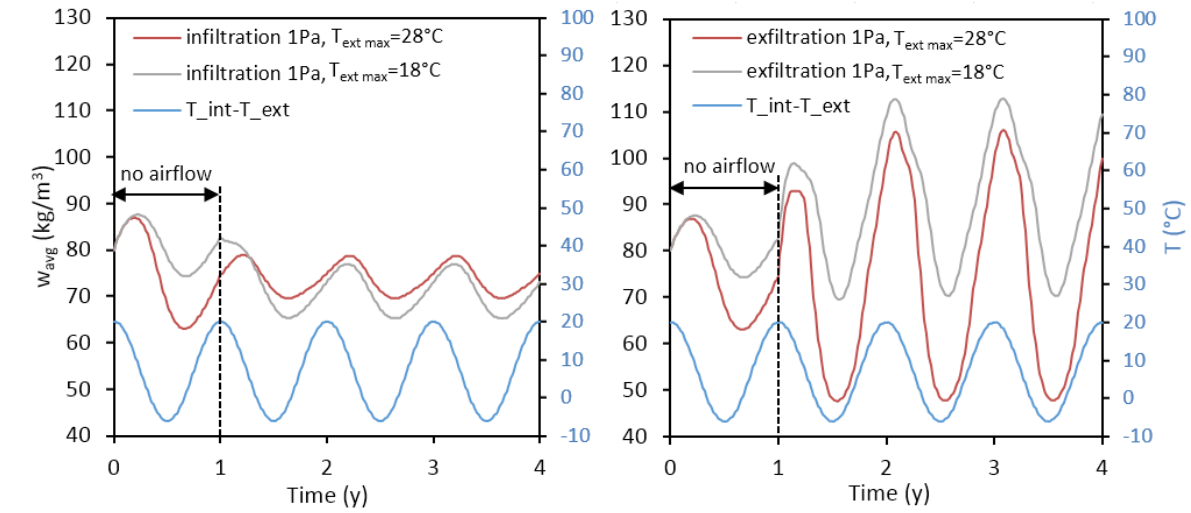

Figure 5: w_{avg} for air infiltration (left) and exfiltration (right), over four years. ΔT with a modified outdoor temperature varying in [0, 28°C] instead of [0, 18°C], is plotted in blue

In order to check the sensitivity of the hygrothermal field to boundary conditions, external temperature variations (fig. 2) have been changed to [0, 28°C] instead of [0, 18°C], the latter designated as the "base case". Variations of w_{avg} in infiltration and exfiltration for $|\Delta P| = 1$ Pa are plotted in (fig. 5). Higher exterior mean temperature together with unchanged exterior relative humidity, result in a more humid exterior air (the exterior vapour pressure has increased). This explains why in infiltration w_{avg} of the modified case is higher than those of the base case. In exfiltration, the assembly is less humidified, as higher temperature level reduces the material relative humidity and thus its moisture content.

4.2 Heat Fluxes

In the following section, the impact of airflow on the hygrothermal field is analysed in term of energy. All heat fluxes included in the energy equation (eq. 1) are evaluated by integrating the respective heat flux densities - q_{cond}; q_{conv}; q_{lat_diff} and q_{lat_adv} - along the interior surface.
Choosing this surface enables to assess the heat transfer between indoor air and the building envelope: the sign of the calculated heat fluxes therefore indicates whether they contribute to heat the interior air (positive flux) or to cool it down (negative flux).
On the 2D section of the defect, the interior surface is composed by five segments (fig. 6). The integration is performed over each segment, what defines a total heat flux:

$$\Phi_{tot} = \int_1 (q_{cond} + q_{lat\_diff}) \cdot \vec{e}_y dx + \int_2 (q_{cond} + q_{conv} + q_{lat\_diff} + q_{lat\_adv}) \cdot \vec{e}_y dx + \int_3 (q_{cond} + q_{lat\_diff}) \cdot \vec{e}_x dy + \int_4 (q_{cond} + q_{conv} + q_{lat\_diff} + q_{lat\_adv}) \cdot \vec{e}_x dy + \int_5 (q_{cond} + q_{lat\_diff}) \cdot \vec{e}_x dy \quad (16)$$

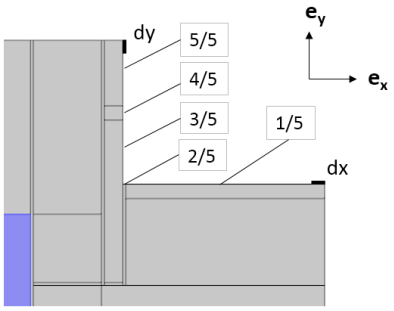

Figure 6: Detail of the five segments composing the interior surface of the assembly

The different heat flux densities have been previously defined in (eqs. 6, 7 and 13). However, the expression of the convective dry air flux and the advective vapour flux will be corrected to the interior conditions, as stated by (eqs. 17 and 18). This does not change the contribution of q_{conv} and q_{lat_adv} in (eq. 1), as only the divergence of these fluxes is needed.

$$q_{conv}(T) = \rho_{air} c_{p_{air}} u (T - T_{int}) \quad (17)$$

$$q_{lat\_adv}(T;\varphi) = L_v[\rho_{vap}(T;\varphi) - \rho_{vap}(T_{int};\varphi_{int})]u \quad (18)$$

Choosing T_{int} and φ_{int} as reference temperature and relative humidity is consistent from building physics perspective, as they are set values to maintain for ensuring thermal and hygric comfort. Hence, an infiltrated airflow injected at T_{int} in the indoor space results in a zero convective heat flux, whereas an infiltrated airflow injected at T_0 with $T_{ext} < T_0 < T_{int}$ represents a deperditive flux equal to $\rho_{air} c_{p_{air}} u(T_0 - T_{int})$, which must be compensated in order to maintain T_{int} in the building. Keeping the same approach for exfiltration, the convective and the advective heat fluxes are zero, as the temperature and relative humidity of the air inlet (located on the interior surface) are imposed at T_{int} and φ_{int} as boundary conditions. This statement is not astounding, as the associated heat loss advected by airflow is already taken into account on the building zone scale, at air inlet locations. Similarly, if the infiltrated airflow contains less moisture than the interior space, i.e. $\rho_0 < \rho_{int}$, this must be

compensated by water vapour generation inside the building zone to maintain the desired humidity, hence a deperditive heat flux equal to $L_v[\rho_{vap}(T_0;\varphi_0) - \rho_{vap}(T_{int};\varphi_{int})]u$.

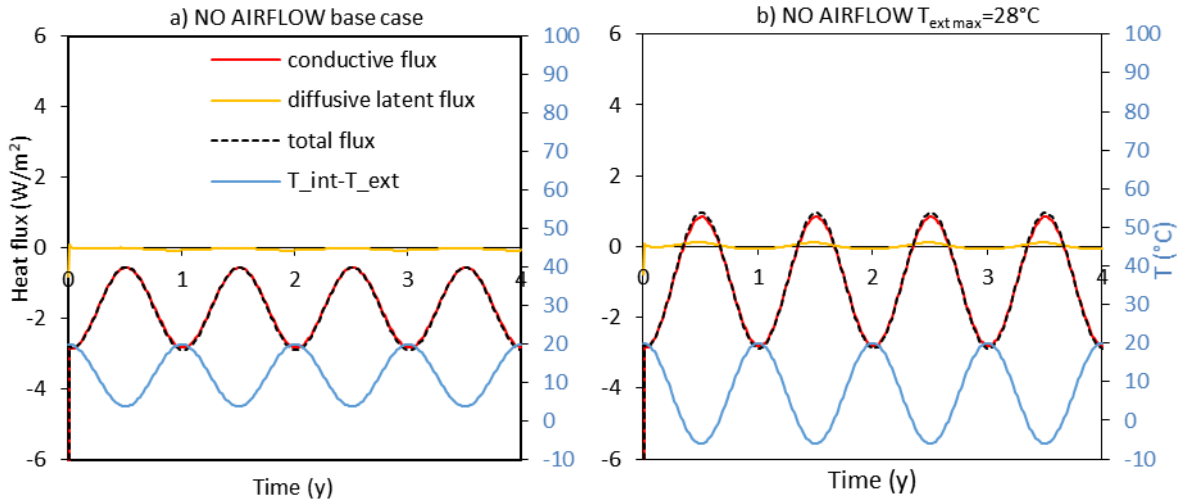

Figure 7: Heat fluxes without airflow over four years, in the base case (a.), in the case of modified $T_{ext\ max}$ (b.)

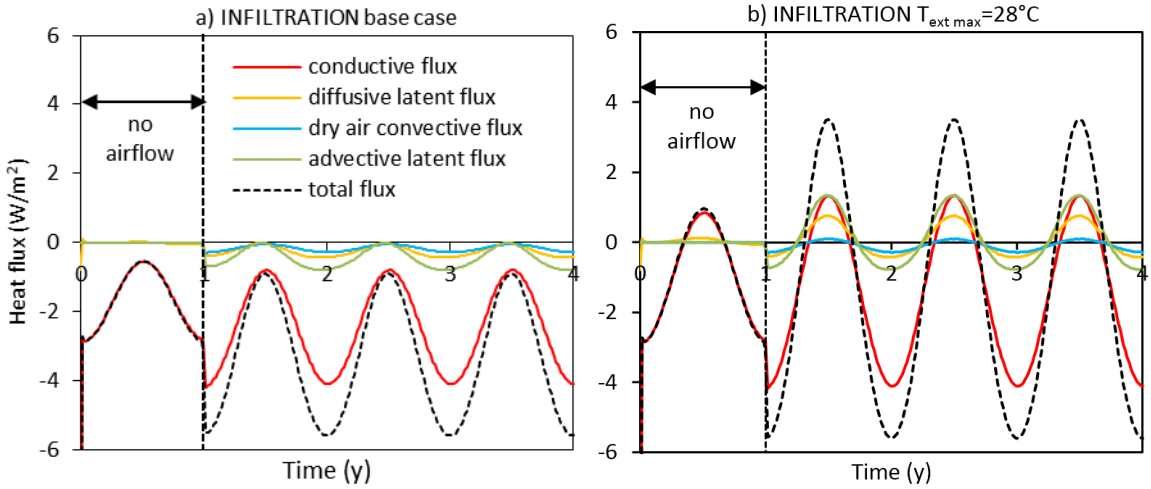

Figure 8: Heat fluxes for the infiltration scenario, in the base case (a.), in the case of modified $T_{ext\ max}$ (b.)

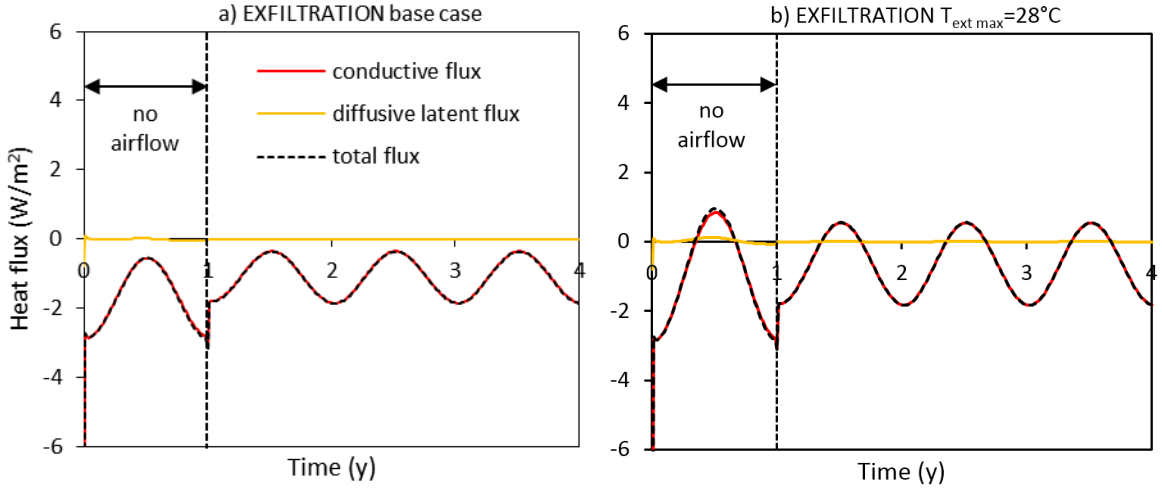

Figure 9: Heat fluxes for the exfiltration scenario, in the base case (a.), in the case of modified $T_{ext\ max}$ (b.)

The heat fluxes are plotted for a 4-year HM simulation without airflow (fig. 7), as well as for infiltration and exfiltration scenarii with $\Delta P = 1$ Pa (figs. 8. and 9. respectively). Contrary to

the moisture response, it appears that even subjected to air transfer, the assembly reaches thermal equilibrium in the first year, which illustrates that heat transfer has much smaller time constants than moisture transfer. The following analysis firstly discusses the base case without airflow, then the impact of infiltration and exfiltration (figs. 7a. 8a. and 9a.). Secondly, the impact of external temperature variation is investigated (figs. 7b. 8b. and 9b.).

Without airflow, in the base case, the total heat loss is mainly constituted by the conductive flux, with a mean value of -1.6 W/m (fig. 7a.). The maximum conductive heat loss is logically attained for the maximum ϕT. The diffusive latent flux is negligible, probably because of the high vapour resistance of the whole multi-layered building assembly.

When air infiltrates at $\phi P = 1$ Pa, the mean conductive heat loss increases to -2.5 W/m (fig. 8a.). This is coherent with the fact that infiltration cools the wall and thus concentrates the temperature gradient in the vicinity of the interior surface, increasing the conductive heat loss. The convective dry air flux is deperditive as well (mean value of -0.17 W/m), as the temperature at the air outlet is lower than T_{int}. Considering latent fluxes, the diffusion flux is still of minor importance (mean value of -0.25 W/m). It is higher than without airflow, as the vapour pressure and temperature gradients are shifted to the interior surface. The advective latent heat flux is a heat loss (mean value of -0.45 W/m), because infiltrated air exiting the interior interface is dryer than ambient air. Overall, the total heat loss in infiltration (mean value of -3.3 W/m) is twice higher than the one without air.

When air exfiltrates, the conductive heat loss decreases to -1.1 W/m (relative to the flux without airflow), as the interior side of the assembly is heated up by the airflow, hence temperature gradient decreases. It is reminded that the convective dry air flux and the advective latent flux are zero according to the choice of T_{int} and $\cdot_{int}$ as reference temperature and relative humidity. The diffusion latent flux is lower than the one in infiltration, because the temperature and vapour pressure gradient are shifted to the exterior side. With this approach, the total heat loss in exfiltration (mean value of -1.1 W/m) is lower than in infiltration or without airflow.

Changing external temperature variation from [0, 18°C] to [0, 28°C], decreases the mean ϕT, hence it lowers the mean conduction heat loss without airflow (fig. 7b.). When T_{ext} is superior to the interior temperature, the heat flux is reversed, turning the heat conduction flux into a heat gain (positive value).

Similarly in infiltration (fig. 8b.), the advective latent heat flux is positive shortly after ϕT is minimal (meaning that $T_{ext} = 28\ ^{\pm}C$ and $T_{int} = 22\ ^{\pm}C$), which indicates that infiltrated air at the interior surface contains more moisture that the indoor air. The modified T_{ext} leads indeed to a more humid exterior air. The diffusive latent heat flux is lower compared to the base case, because the vapour pressure gradient between indoor and outdoor is lower.

In exfiltration (fig. 9b.), the effect of the reduced temperature gradient appears clearly, similarly to the case without airflow (fig. 7b.).

5 CONCLUSION

A numerical model for simulating HAM transfer through complex wall assemblies including permeable porous material and thin air channels has been presented. This tool has been used to assess the impact of leaking air on the hygrothermal field in an airtightness defect, subjected to classical boundary conditions. Additional moisture risk is expected in case of air exfiltration, whereas air infiltration has a drying effect on the assembly. Higher external temperature slightly increases moisture storage in infiltration, and reduces it in exfiltration. An approach to calculate sensible and latent heat fluxes through the defect is proposed. To obtain more quantitative results about the energy impact of air leakage, it seems relevant to consider the building zone scale, where airtightness defects, air inlet and outlet can be combined. This could be the aim of further research work.

6 ACKNOWLEDGEMENTS

This work is financially supported by the French Environment and Energy Management Agency (ADEME), the Building Scientific and Technical Centre (CSTB), the French National Agency (ANR) through its Sustainable Cities and Building programme (MOB-AIR project n°ANR-12-VBDU-0009), and the Région Rhône-Alpes.

7 NOMENCLATURE

u [m/s]	air velocity	$\pm_{mat}$ [kg=(s:m:Pa)]	vapour permeability of material
k_{mat} [m^2]	intrinsic permeability of material	$\frac{1}{2}_{mat}$ [kg/ m^3]	dry density of material
$'_{air}$ [Pa.s]	dynamic viscosity of dry air	$\bar{}$ [kg/(s.m^2.K)]	moisture surface film coefficient
$\frac{1}{2}_{air}$ [kg/m^3]	dry air density	h [W/(m^2.K)]	heat surface film coefficient
$c_{p_{air}}$ [J/(kg.K)]	specific heat of dry air	L_v [J/kg]	vapour latent heat of sorption
c_{mat} [J/(kg.K)]	spec. heat of dry material	D_w [m^2/s]	moisture diffusivity
c_w [J/(kg.K)]	spec. heat of liquid water	R [J/(mol.kg)]	universal gas constant
^{1} [¡]	vapour resistance factor of material	M_w [kg/mol]	molar mass of water
H [kg=m^3]	specific enthalpy	P [Pa]	total air pressure

8 REFERENCES

Belleudy, Clément. 2015. “Modélisation Des Transferts D’air et Leur Impact Sur Le Comportement Hygrothermique Des Bâtiments.” Ph.D. Thesis, Univ. Grenoble Alpes.

Belleudy, Clément, Ahmad Kayello, Monika Woloszyn, Hua Ge, Paul Fazio, Marx Chhay, and Daniel Quenard. 2014. “A Heat-Airflow Model for Simulating the Effects of Air Leakage on the Temperature Field in Porous Insulation.” In *10th Nordic Symposium on Building Physics*, 79–86. Lund, Sweden.

Buchanan, C. R., and M. H. Sherman. 2000. “A Mathematical Model for Infiltration Heat Recovery.” Lawrence Berkeley National Laboratory.

CETE de Lyon. 2010. “Carnets Prebat Mininfil, Mémento Étanchéité - Construction Ossature Bois - Isolation Thermique Intégrée.”

Janetti, Michele Bianchi. 2014. “Assessment of the Moisture Risk in Constructions Including Convection inside Air Cavities.” In *10th Nordic Symposium on Building Physics*, 1038–44. Lund, Sweden.

Janssens, A. 1998. “Reliable Control of Interstitial Condensation in Lightweight Roof Systems: Calculation and Assessement Methods.” Ph.D. Thesis, Departement of Civil Engineering, KU Leuven, Belgium.

Künzel, H.M. 1995. “Simultaneous Heat and Moisture Transport in Building Component.” Fraunhofer IBP.

Langlais, Catherine, Eric Arquis, and Dave J. McCaa. 1990. “A Theoretical and Experimental Study of Convective Effect in Loose-Fill Thermal Insulation.” *Insulation Materials: Testing and Applications, ASTM STP 1030*, 290–318.

Langmans, Jelle. 2013. “Feasibility of Exterior Air Barriers in Timber Frame Construction.” Ph.D. Thesis, Departement of Civil Engineering, KU Leuven, Belgium.

Nespoli, Lorenzo, M. Bianchi Janetti, and Fabian Ochs. 2013. “Comparing Different Approaches for Moisture Transfer inside Constructions with Air Gaps.” In *COMSOL Conference Rotterdam*.